HYDROSTATIC PRESSURE EFFECT ON THE GUNN THRESHOLD ELECTRIC FIELD In n-InSb

by

NIZAM UDDIN AHMAD

A Thesis submitted in partial fulfillment
of the requirements for the Degree of
Master of Science.

Department of Physics,
Lakehead University,
Thunder Bay, Ontario, Canada.

May, 1978.

ProQuest LLC.
789 East Eisenhower Parkway
P.O. Box 1346
Ann Arbor, MI 48106 - 1346

"This Thesis is dedicated to my mother and father".

ACKNOWLEDGEMENTS

It gives me great pleasure to thank Dr. W. J. Keeler, my research supervisor, for his generous and instructive help throughout this project.

Special thanks are due to Mrs. M. Hawton for her helpful discussions concerning the data analysis.

I wish to express my appreciation to Mr. G. C. Anderson for assisting in the construction and maintenance of the cryostats, to Dr. R. E. Jones for comments on the thesis and to Dr. V. V. Paranjape for his interests in the research project.

The co-operation from my colleague, Mr. S. M. Fong, in using the apparatus is gratefully acknowledged.

I also wish to thank my brother, Mr. Z. U. Ahmad, for his constant encouragement from Pakistan throughout this work.

Finally, I wish to express my thanks to Mrs. J. Parnell for typing my thesis.

ABSTRACT

The Gunn effect as a function of pressure has been studied in n-type InSb. The Gunn threshold field is found to decrease with increasing pressure reaching a minimum at P ≈ 9 kbars. It then increases while the oscillations weaken with increasing pressure up to 12 kbars. Low field Hall and conductivity measurements have also been made in an attempt to obtain a possible explanation for the threshold minimum. It is observed that the impurity level moves away from the conduction band approximately exponentially with increasing pressure. By 9 kbars the donor ionization energy is large enough that considerable freeze-out or deionization of donor states occurs. The reduction in carrier number is unfavourable to the Gunn process and hence leads to an increase in the threshold field for pressures above 9 kbars.

TABLE OF CONTENTS

LIST OF FIGURES

List of Figures continued...

INTRODUCTION

At atmospheric pressure the lowest conduction band minimum in InSb is centred at the Γ point and the energetic distance to the higher L minima is greater than the direct energy gap from the valence to conduction band of about 0.2 ev. Initially it was thought that if a uniform electric field of a few hundred volts/cm was applied to n-type InSb, the dominant effect would be the creation of electron-hole pairs due to bulk avalanche instead of carrier transfer from the Γ to L band with consequent possible observation of the Gunn effect. However, in 1969, Porowski and co-workers[1] observed the Gunn effect in n-InSb at 77K and high pressure. Also Smith and co-workers[2] found that for very short times (<1 nanosec) after the application of an electric field pulse, the Gunn effect could be identified at zero pressure and 77K. Pressure leads to a stablization of the effect because it increases the valence to Γ conduction band gap E_g and at the same time decreases the inter-conduction band gap $E_{\Gamma L}$. In reporting the results of their pressure investigation, they noted that their samples gave rise to two types of behaviour. Type A samples, whose properties they did not specify, showed a reduction in the Gunn threshold field E_{th} with increasing pressure up to a pressure of about 9 kbars where a minimum occurred. For higher pressures E_{th} increased and the Gunn oscillations weakened.

Type B samples, again unspecified as to impurity concentration and other properties, showed a monotonic reduction in E_{th} up to a pressure of approximately 12 kbars and no noticeable weakening in the Gunn oscillations. They suggested carrier freeze-out as a possible explanation for the behaviour of their type A samples. Similar work by Dobroval'skis and coworkers[3] on n-InSb samples of known carrier concentration at 77K showed only a monotonic reduction in E_{th} with increasing pressure.

Because of the two dissimilar behaviour patterns and relatively poorly understood properties of the samples so far investigated, it was decided that joint Gunn effect and Hall measurements would be carried out on samples from the same InSb monocrystal. This thesis reports on some of the results of these measurements.

Measurements were carried out on n-InSb samples with an electron density $n = 8.4 \times 10^{13}$ cm^{-3} and mobility $\mu = 60$ m^2 V^{-1} sec^{-1} at liquid-nitrogen temperature and zero pressure. In Chapter I we have briefly presented a description of the Gunn effect. Also, using the assumption that a parabolic relation exists between energy and momentum in InSb, the relations for the temperature dependent carrier concentration in the intrinsic and extrinsic ranges of semiconductor behaviour are reviewed. In Chapter II equipment and experimental methods are discussed. Results are presented and analyzed in Chapter III. Chapter IV presents the conclusions.

CHAPTER 1

THEORETICAL DISCUSSION

1:1 Band Structure in InSb

InSb is one of those materials for which a reasonable amount of reliable band structure information is available. The conduction band in InSb consists of two sub-bands of interest for the present investigation. The minimum of the conduction band lies at the centre of the Brillouin zone (Γ point). The next higher band is centred at the L symmetry point. The Γ to L conduction band gap is larger than the valence to conduction band gap at $\vec{k} = 0$.

Kane[4] obtained a set of $E(\vec{k})$ relations for III - IV direct gap semiconductors applicable to InSb. Measuring energy from the top of the valence band, he obtained the relationships for the Γ conduction band and the various hole bands. The conduction band relationship is given by:

$$E - E_g = \frac{\hbar^2 k^2}{2m_o} + \frac{1}{2}\left(\sqrt{E_g^2 + \frac{8p^2k^2}{3}} - E_g\right). \qquad 1.1$$

The heavy hole valence band relationship is:

$$E = \frac{-\hbar^2 k^2}{2m_o} , \qquad 1.2$$

the light hole band relationship is:

$$E = \frac{-\hbar^2 k^2}{2m_o} - \frac{1}{2}\left(\sqrt{E_g^2 + \frac{8p^2k^2}{3}} - E_g\right) , \qquad 1.3$$

and the split-off valence band relationship is:

$$E = -\Delta - \frac{\hbar^2 k^2}{2m_o} - \left\{\frac{p^2k^2}{3E_g+3\Delta}\right\} . \qquad 1.4$$

In the above equations m_o is the free electron mass, Δ is the spin-orbit splitting energy at $\vec{k} = 0$, and p is a parameter to be determined by the experimental value of the effective mass m_Γ at the bottom of the conduction band. If energy E' is measured from the bottom of the conduction band, and if the term $\hbar^2k^2/2m_o$ is ignored since $m_o \simeq 80m_n^*$, then the conduction band may be represented by:

$$E' = \frac{1}{2}\left(\sqrt{E_g^2 + \frac{8p^2k^2}{3}} - E_g\right). \qquad 1.5$$

Defining the effective mass to be:

$$m_n^* = \frac{3\hbar^2 E_g}{4p^2} \qquad 1.6$$

one obtains:

$$\frac{\hbar^2 k^2}{2m_n^*} = E' \left(1+\frac{E'}{E_g}\right) \qquad 1.7$$

which is hyperbolic relation between E' and k. Provided the conduction band is not too full ($E' < E_g$), this equation reduces to a parabolic relation:

$$E' = \frac{\hbar^2 k^2}{2m_n^*} . \qquad 1.8$$

Pressure increases the energy gap E_g and hence the effective mass m_n^*. Since the density of states in a parabolic band is proportional to $m_n^{*3/2}$, increasing pressure improves the parabolic band assumption both through density of states and E'/E_g variation. The L conduction band is known to be approximately 0.45 eV above the bottom of the Γ conduction band[5]. Estimates of pressure derivatives for E_g and $E_g + E_{\Gamma L}$ are 14×10^{-3} eV/kbar (experimental)[6] and 8.3×10^{-3} eV/kbar (calculated)[7], respectively. Thus, $E_{\Gamma L}$ should decrease with increasing pressure at a rate of about -6×10^{-3} eV/kbar. The pressure dependent band structure of InSb is shown in Fig. I.1.

FIGURE 1.1 The Band Structure of InSb. The Dashed Line Shows Band Structure at P ≃ 15 kbars.

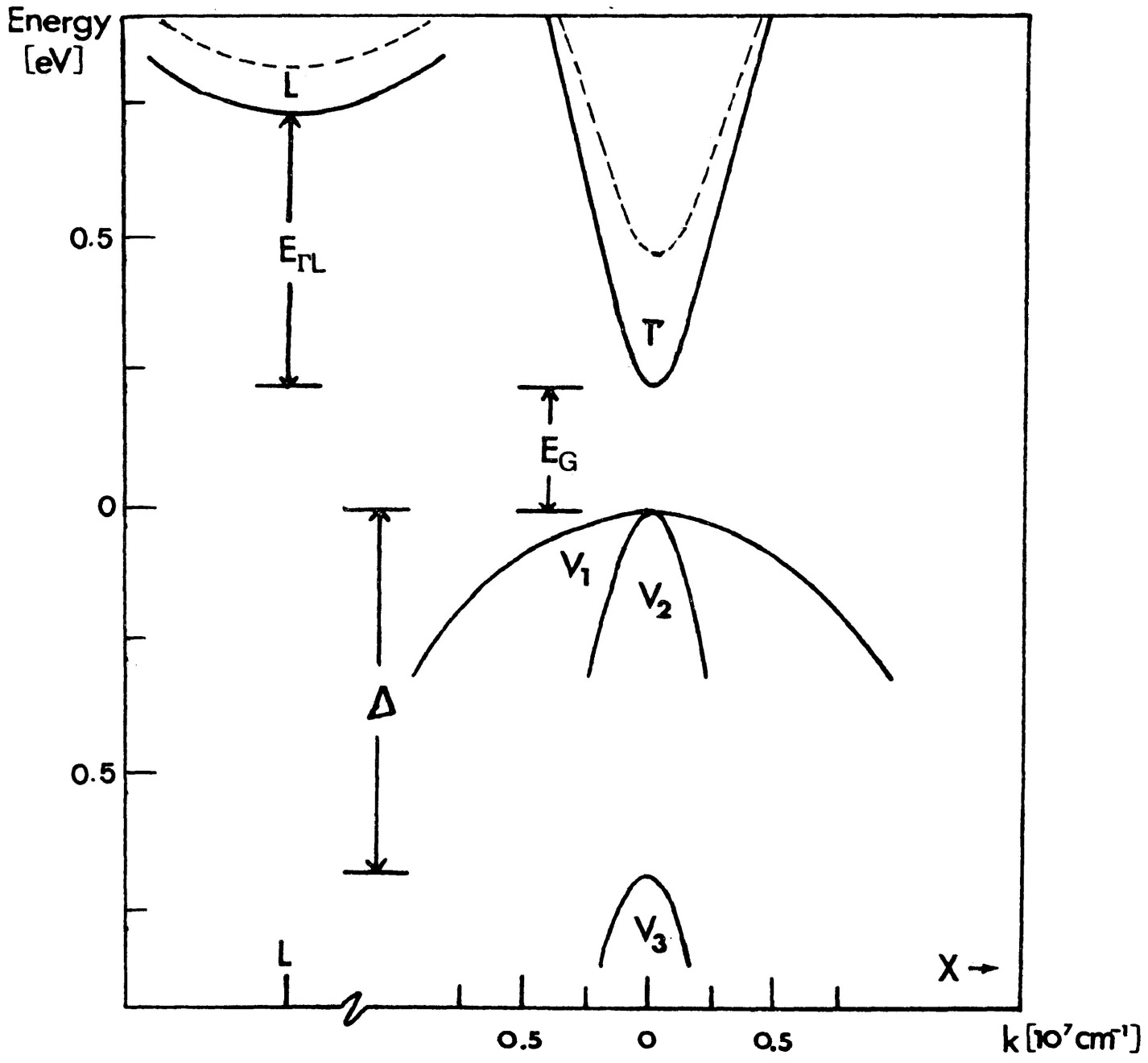
Energy
[eV]
L
$E_{\Gamma L}$
Γ
E_G
0.5
0
0.5
V_1
V_2
Δ
V_3
L
X
0.5
0
0.5
k [10^7 cm^{-1}]

I.2a Qualitative Description of the Gunn Effect

The Gunn effect is a carrier transit time effect which can be qualitatively explained in the following way. If the conduction band of a material consists of portions with two widely differing mobilities, as for example in the Γ and L bands of InSb where $\mu_\Gamma/\mu_L >> 1$, it may be possible with the application of an electric field to produce a negative differential conductivity (NDC), that is, there may be a reduction in I for an increase in V. The electric field increases the energy of the carriers and these heated electrons may be transferred to the higher energy, low-mobility L band. The transfer rate will be proportional to exp $-(E_{\Gamma L}/kT_e)$ where T_e is the electron temperature. Once a significant number of electrons are in the L band where their mobility is drastically reduced, the conductivity of the sample $\sigma = e(n_\Gamma\mu_\Gamma + n_L\mu_L)$ will decrease as the factor n_L/n_Γ increases.

In order to see how this leads to the production of domains which are interpreted as "oscillations", consider the effect of the two conduction band contributions on the sample current. At low electric fields the sample conductivity is determined by the Γ conduction band. As the field is increased, eventually some electrons are transferred to the low-mobility L band, and a part of the sample

behaves as though its conductivity is given by that of the L conduction band. Depending on the load line slope, the actual operating condition for the sample will consist of a certain fraction of the electrons in the Γ conduction band and the rest in the L conduction band. The highest electric field region is usually near an edge or at a sample flaw so the L band behaviour first appears at one of these. Let us assume this corresponds to a region close to the cathode end of the sample. A time-space analysis of the sample now leads to the following type of plot of electric field $|\vec{E}|$ and charge density ρ as a function of position along the sample.

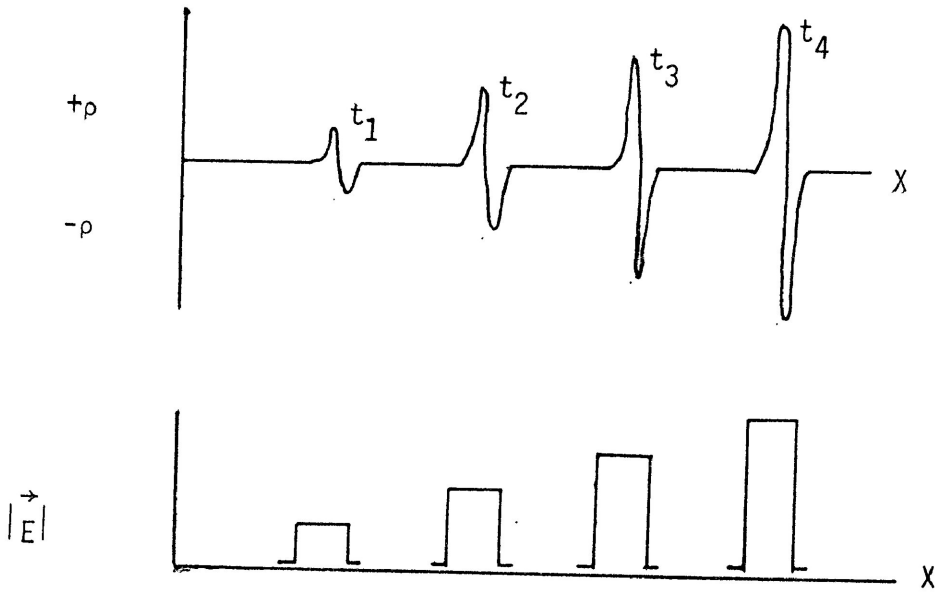

FIGURE I.2. The electric field $|\vec{E}|$ and charge density ρ as a function of position along the sample at different times.

In the region of high local field some electron transfer to the L band occurs and the electrons become less mobile than the electrons in the neighbouring lower field regions. This means electrons enter and leave this sample region faster than they drift through it. Thus, the charge density variation associated with the initial local high electric field is amplified, producing a higher local electric field region. As the "domain" grows in amplitude, it also drifts towards the anode with the Γ band mobility which leads to the time sequence of events shown. In the sample region through which the domain has passed, the electric field is reduced because the electric field in the domain may have been several thousands of volts per cm and therefore sufficiently high to produce bulk avalanche pair-creation. Energy density considerations then require $|\vec{E}|$ to decrease in this region of excess conductivity in the wake of the Gunn domain.

When the domain arrives at the anode a pulse of charge and a short term high electric field is produced. The sample recovers as the avalanche pairs recombine and the process starts over again provided the sample geometry meets the appropriate circuit requirements. Periodic arrival of domains at the anode results in an apparent oscillation in the anode potential.

I.2b Condition for NDC in Interband Gunn Oscillators

For a calculation of the condition necessary for the NDC, we follow the treatment given by Hilsum.[8] We assume equal electron temperatures in the high and low mobility bands, for example, the Γ and L bands in InSb. The ratio of electron densities, $\eta = n_\Gamma/n_L$ is given by the ratio of the densities of states, $N_{c\Gamma}/N_{cL}$, and the difference between the two sub-band energies, $E_{\Gamma L}$, such that:

$$\eta = \left(\frac{N_{c\Gamma}}{N_{cL}}\right) \exp\left(\frac{E_{\Gamma L}}{K_B T_e}\right). \qquad 1.10$$

For $n = n_\Gamma + n_L$, one may write

$$n_\Gamma = n\eta/(1+\eta)$$

and $n_L = n/(1+\eta)$.

The conductivity is given by:

$$\sigma = e\,(n_\Gamma \mu_\Gamma + n_L \mu_L) \qquad 1.11$$

$$= e\, n\, \mu_L \frac{(\eta b+1)}{(\eta+1)}, \qquad 1.12$$

where $b = \mu_\Gamma/\mu_L$ is the mobility ratio. For a voltage V applied to a

filamentary sample of length L and area A, the current $I = \sigma AV/L$ versus V has a slope given by:

$$\frac{dI}{dV} = \left(\frac{A}{L}\right)\left(\sigma + V\frac{d\sigma}{dV}\right)$$

$$= \left(\frac{A}{L}\right)\sigma\left\{1 + \frac{\vec{E}}{\sigma}\left(\frac{d\sigma}{d|\vec{E}|}\right)\right\} \qquad 1.13$$

$$= \left(\frac{A}{L}\right) n|e|\mu_L \left(\frac{nb+1}{n+1}\right)\left\{1-\frac{n(b-1)}{(n+1)(nb+1)}\right. \quad \left.\frac{E_{\Gamma L}|\vec{E}|}{K_B T_e^2}\right. \quad \left.\frac{dT_e}{d|\vec{E}|}\right.$$

The sign of dI/dV depends strongly on $dT_e/\, d|\vec{E}|$. NDC is achieved when dI/dV is negative. Since the quantities n, b, and $E_{\Gamma L}$ are pressure dependent, the NDC is also pressure sensitive.

1.3 Low Electric Field Properties of InSb

With the assumption that a parabolic relation, $E(\vec{k}) = \hbar^2\vec{k}^2/2m_n^*$, holds true for sufficiently low electron energies in InSb, we present a review of the carrier density in the InSb conduction band in the intrinsic and extrinsic limits. The density of states in a parabolic conduction band is given by:

$$g(E)\,dE = 2\left(\frac{V}{4\pi^2}\right)\left(\frac{2m_n^*}{\hbar^2}\right)^{3/2}(E - E_c)^{1/2}\,dE \qquad 1.14$$

where V is the crystal volume. The total concentration of the carriers in the conduction band is then given by:

$$n = \frac{1}{V} \int_{E_c}^{\infty} f(E)\, g(E)\, dE, \qquad 1.15$$

where f(E) is the Fermi-Dirac distribution function. Substitution of Eqn. I-14 into I-15 gives:

$$n = \frac{2}{4\pi^2} \left(\frac{2m_n^*}{\hbar^2}\right)^{3/2} \int_{E_c}^{\infty} \frac{(E - E_c)^{1/2}\, dE}{\{\exp\left(\frac{E-\xi}{k_B T}\right) + 1\}} \qquad 1.16$$

$$= N_c\, F_{1/2}\, (\xi_n / k_B T), \qquad 1.17$$

where $\xi_n = \xi - E_c$, N_c is the effective density of states given by:

$$N_c = 2 \left(\frac{m_n^*\, k_B T}{2\pi\hbar^2}\right)^{3/2} \qquad 1.18$$

and the Fermi integral is given by:

$$F_j(\eta) = \frac{1}{j!} \int_0^\infty \frac{x^j \, dx}{\exp(x-\eta) + 1} . \qquad 1.19$$

This integral reduces to $\exp(\eta)$ for $\eta < -4$, the non-degenerate limit.

I.3a Intrinsic Case

In the intrinsic case the electron density n is equal to the hole density p. From the law of mass action:

$$n = (np)^{1/2} = (N_c N_v)^{1/2} \exp(-E_g/2k_BT)$$

$$= 2 \left(\frac{k_BT}{2\pi\hbar^2}\right)^{3/2} (m_n^* m_p^*)^{3/4} \exp\left(\frac{-E_g}{2k_BT}\right) . \qquad 1.20$$

The energy gap E_g is usually found to vary linearly with temperature.[10] We therefore write:

$$E_g = E_{go} - \alpha T . \qquad 1.21$$

The temperature coefficient $(\partial E_g/\partial T)_{p=o}$ has been estimated for InSb.

Using an extrapolated value of E_{go} = 0.27 eV[11] and room temperature value of E_g (296K) = 0.18 eV, one obtains $\alpha \simeq 3 \times 10^{-4}$ eV/K. Substituting Eqn. I-21 into Eqn. I-20, one obtains:

$$\left(\frac{n}{T^{3/2}}\right) = 2\left(\frac{4\pi^2 m_n^* m_p^*}{h^2}\right)^{3/4} \exp\left(\frac{\alpha}{2k_B}\right) \exp\left(\frac{-E_{go}}{2k_B T}\right). \quad 1.22$$

A semilogarithmic plot of $(n/T^{3/2})$ vs 1/T should show a linear relationship. The slope will be used to determine E_{go}, the energy gap at T = 0. The effective mass m_n^* and energy gap E_g are pressure sensitive. Differentiating $\ell n\ n$ with respect to P one obtains:

$$\frac{d(\ell n\ n)}{dP} = \frac{3}{4}\ \frac{d(\ell n\ m_n^*)}{dP} - \frac{1}{2k_B T}\ \frac{dE_g}{dP}, \quad 1.23$$

assuming $d\ell n\alpha/dP \simeq 0$.

For low electric fields $\mu_p << \mu_n$, thus $\rho = (ne\mu_n)^{-1}$ and we can write:

$$\frac{d(\ell n\ \rho)}{dP} = \frac{1}{2K_B T}\ \frac{dE_g}{dP} - \frac{3}{4}\ \frac{d(\ell n\ m_n^*)}{dP} - \frac{d(\ell n\ \mu_n)}{dP}. \quad 1.24$$

1.3b Extrinsic Case for n-Type Material

An analysis of carrier concentration in the conduction band of n-type material for the low temperature extrinsic limit is complicated by the presence of acceptors which results in compensation. Seeger[12] has given a treatment of this problem. Provided one considers the non-degenerate case, which is true for pressure greater than about 5 kbars in InSb, the following relation holds:

$$\frac{n\ (n+N_A)}{N_D-N_A-n} = \frac{N_c}{g_D}\ \exp\ (^{-E_D/k_BT}) \qquad 1.25$$

where n is the conduction band electron concentration, N_A is the number of acceptors per unit volume, N_D is the number of donor atoms per unit volume, N_C is the conduction band density of states and g_D accounts for possible multiplicity in impurity atom bound states.

For pure (undoped) n-type material $N_A << N_D$ and, provided that $N_A < n$, one obtains

$$\frac{n^2}{N_D-n} = \frac{N_c}{g_D}\ \exp\ (\frac{-E_D}{k_BT}). \qquad 1.26$$

Since $N_c = 2\ (m_n^*\ k_BT/2\pi\hbar^2)^{3/2}$ for a parabolic conduction band, the following equation holds:

$$\frac{d \ln \left(\frac{n^2}{(N_D - n)\, T^{3/2}} \right)}{d \left(\frac{1}{T} \right)} = \frac{-E_D}{k_B} . \qquad 1.27$$

Thus, one may determine E_D, the donor ionization energy, by measuring n for a range of extrinsic temperature behaviour.

CHAPTER 2

EXPERIMENTAL METHODS

Pressure investigations of the Gunn and Hall effects were carried out separately.

2:1a Gunn Effect Measurements

The experimental arrangement is shown schematically

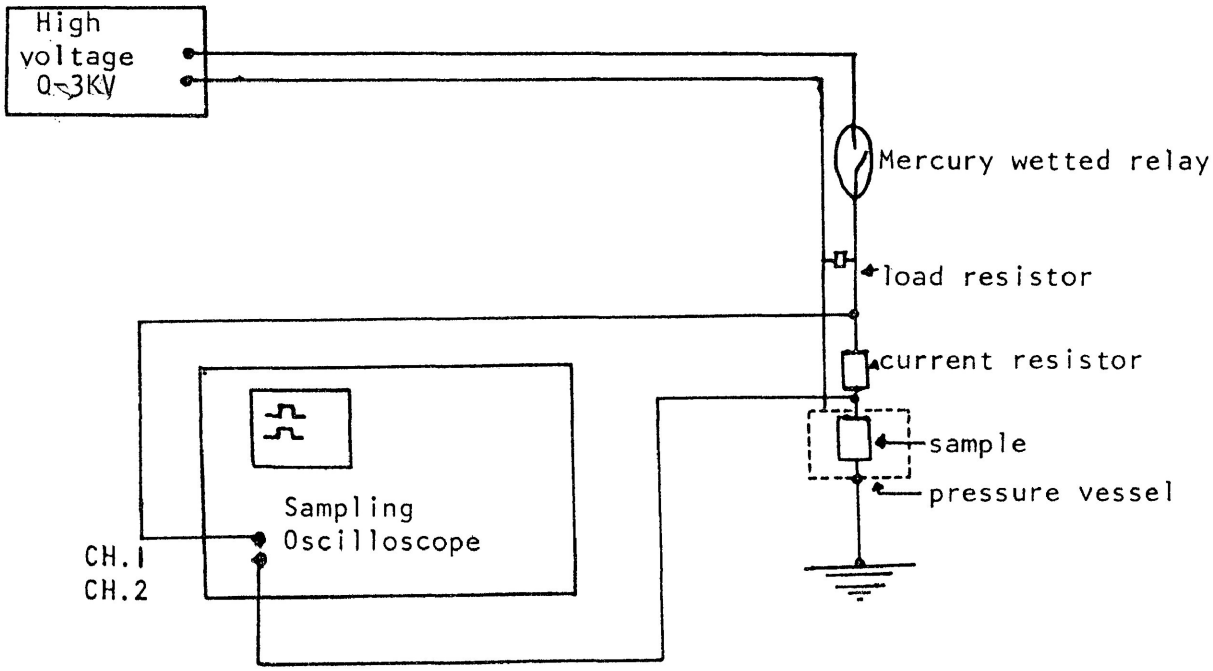

FIGURE 2.1 Schematic Arrangement for the Gunn Effect Study

The sample was placed in a pressure vessel and pressure was applied by means of a hydraulic system. To create a short fast rise-time pulse, a strip transmission line was charged to a potential V and discharged through a mercury wetted relay. The pulse was then carried by a second identical line to the sample through the pressure feed-through. The voltage across the sample was monitored on one channel of a two channel sampling oscilloscope. The current through the sample was obtained by measuring the voltage across a ½ Ω resistor in series with the sample. This was displayed on channel two of the oscilloscope. From current and voltage vs time data, current vs voltage information at different times was obtained.

2.1b High Pressure Apparatus

A double walled piston and cylinder vessel[13] with pressure capabilities to 30 kbars was used for pressurizing the sample. Force was applied to the pressure vessel by means of a press frame actuated by a hand operated hydraulic pump (Fig. 2.2). Details of the high pressure chamber are shown in Fig. 2.3. Except for the tungsten carbide thrust piston, all parts of the pressure vessel were made of Be-Cu 25 which is non-magnetic, has good thermal conductivity and is one of the strongest non-brittle metals under

FIGURE 2.2 High-Pressure Cryostat and External Hydraulic System

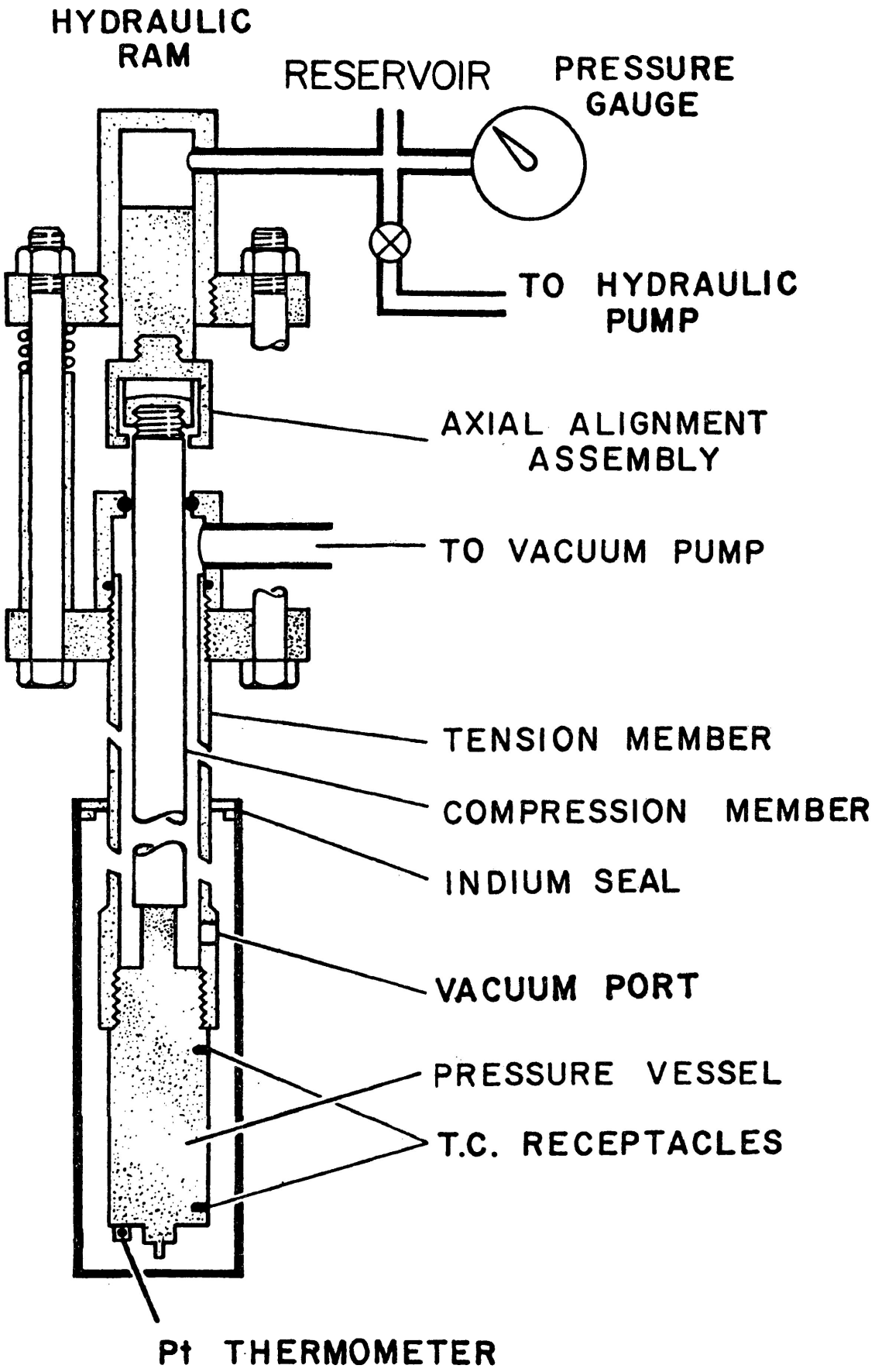
HYDRAULIC RAM
RESERVOIR
PRESSURE GAUGE
TO HYDRAULIC PUMP
AXIAL ALIGNMENT ASSEMBLY
TO VACUUM PUMP
TENSION MEMBER
COMPRESSION MEMBER
INDIUM SEAL
VACUUM PORT
PRESSURE VESSEL
T.C. RECEPTACLES
Pt THERMOMETER

FIGURE 2.3 High Pressure Vessel with Self Stressing Double-Walled Cylinder

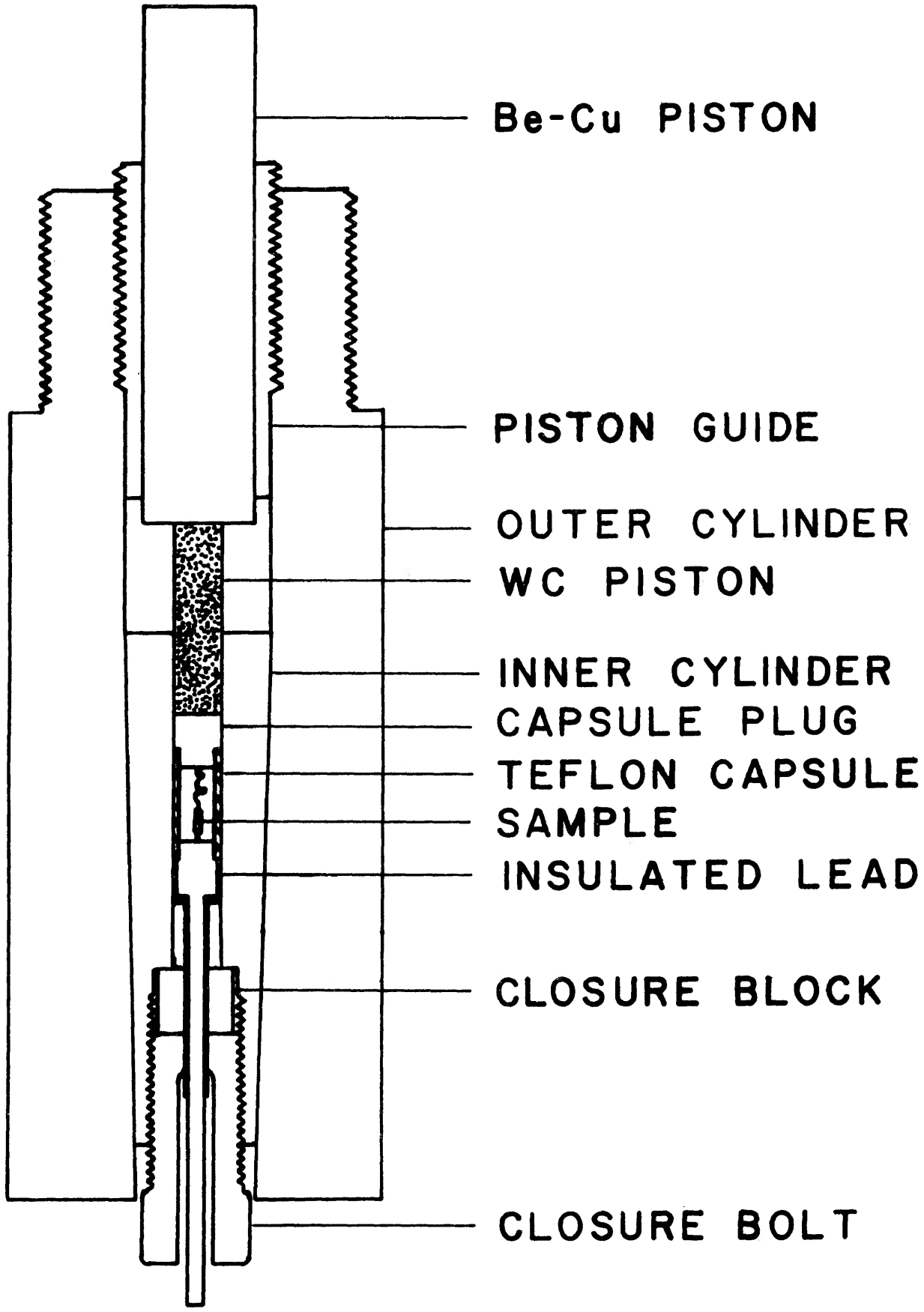
Be-Cu PISTON
PISTON GUIDE
OUTER CYLINDER
WC PISTON
INNER CYLINDER
CAPSULE PLUG
TEFLON CAPSULE
SAMPLE
INSULATED LEAD
CLOSURE BLOCK
CLOSURE BOLT

cryogenic conditions. The electrical feed-through supports the sample inside a Teflon capsule filled with a pressure transmitting liquid (1:1 mixture of isoamyl-alcohol and n-Pentane). This capsule is closed at the upper end by a ½ hard Be-Cu plug. The pressure vessel was pressurized to the desired pressure and then cooled to 77K by submersion in liquid nitrogen.

2.1c The Pulse System

A pulsed electric measurement requires an electric feed-through into the pressure vessel with an impedance matched to the external line.

A low impedance strip transmission line was used to deliver high energy pulses to the sample. The stripline was fabricated from materials obtained from Pampus Fluoroplast, W. Germany. The stripline consists of a 0.38 mm Teflon sheet covered on both sides by 0.22 mm thick high conductivity copper. With the assumption that medium permeability μ is equal to the vacuum permeability μ_0, the transmission line parameters are given in MKS units by[14]

$$L = 4\pi x 10^{-7}\ b/a \quad \text{henries/meter},$$

$$C = \frac{1}{36\pi} \times 10^{-9} (a/b)\varepsilon_r \text{ farads/meter}$$

and $$Zo = \frac{120\pi}{\sqrt{\varepsilon_r}} (b/a) \text{ ohms,}$$

where $\varepsilon_r = \varepsilon/\varepsilon_o$

a = width of the transmission line and

b = separation distance (dielectric filled).

Since ε_r (Teflon) = 2.1, it was possible to have a transmission line with low impedance, the value depending on the ratio of a to b.

The parameters of the transmission line used in this study were:

a/b = 30,

$L = 4.19 \times 10^{-8}$ henries/meter,

$C = 5.6 \times 10^{-10}$ farads/meter and

$Z_o = 8.7$ ohms.

A stepped feed-through[15] with magnesia-filled epoxy insulation (Fig. 2.4) was used to transmit energy into the sample from the stripline. The important parameters of the coaxial feed-

through were obtained from the following relations:

$$L = \frac{\mu}{2\pi} \ln\left(\frac{b}{a}\right) \text{ henries/meter,}$$

$$C = \frac{2\pi\varepsilon}{\ln(b/a)} \text{ farads/meter and}$$

$$Z_o = \frac{60}{\sqrt{\varepsilon_r}} \ln\left(\frac{b}{a}\right) \text{ ohms,}$$

where $\mu \simeq \mu_o$, $\varepsilon = \varepsilon_o \varepsilon_r$, and a and b are inner and outer radii of the coaxial line, respectively. The dielectric constant of the MgO-filled epoxy used in this experiment was 2.63. Using this value and b/a = 1.254 we obtained $Z_o \simeq 8.4$ ohms.

The feed-through, in series with an external ½ Ω current measuring resistor, was connected across one end of the stripline. The pulse generator was connected to the other end of this stripline. Since the sample resistance was expected to change (3-30 Ω) with rising pressure, a 3 Ω resistor was connected in parallel across the sample and current measuring resistor to provide a nearly constant load impedence of 3 Ω.

Voltages across the sample and the current measuring resistor were picked off using 50 Ω coaxial lines and fed to a sampling scope.

FIGURE 2.4 Inner Cylinder of a Self-Stressing Double-Walled Pressure Vessel Showing Detail of the Low-Impedance Feed Through Used for Transmission of Nanosecond Pulses. (Dimensions are in Millimeters)

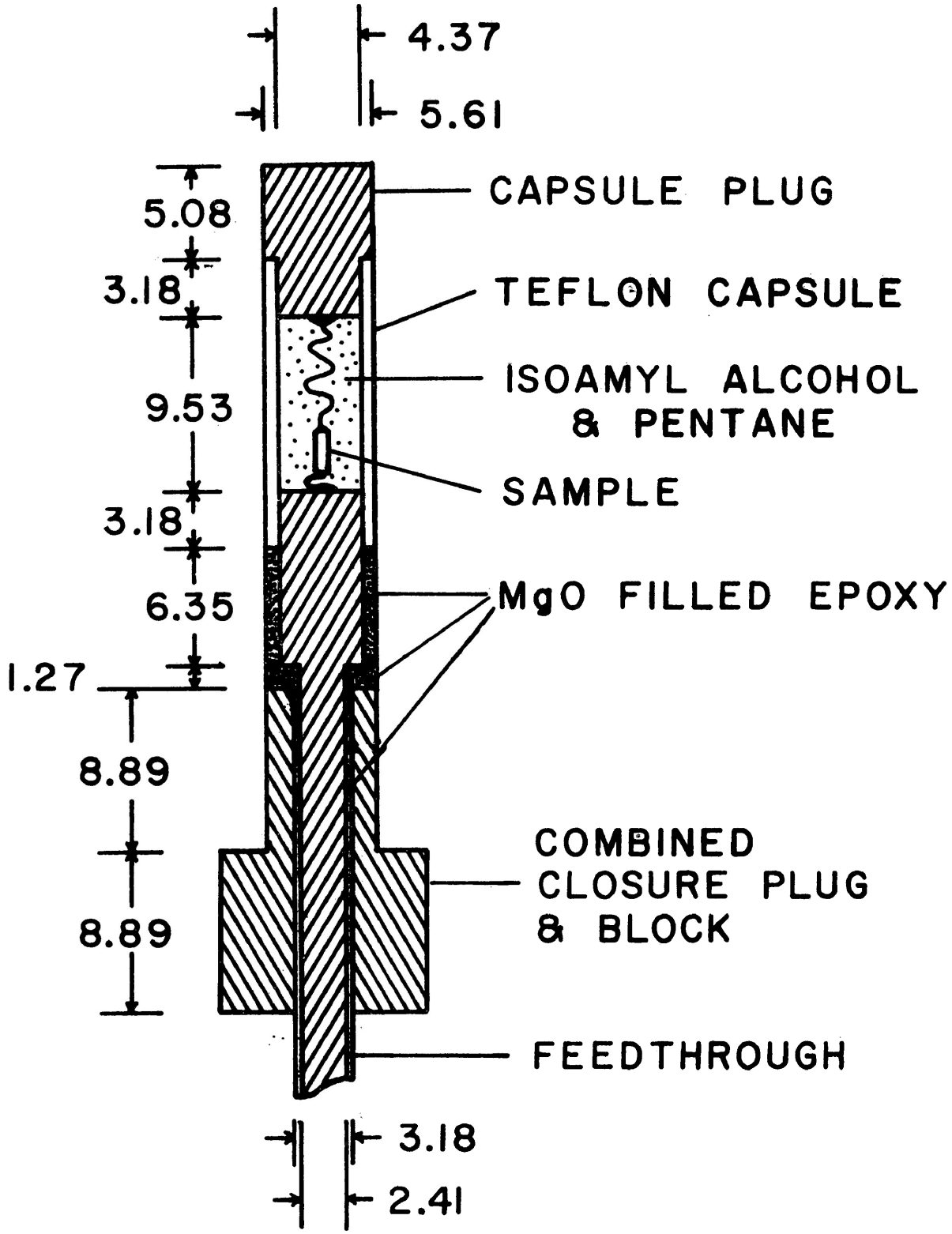
4.37
5.61
5.08
3.18
9.53
3.18
6.35
1.27
8.89
8.89
CAPSULE PLUG
TEFLON CAPSULE
ISOAMYL ALCOHOL
& PENTANE
SAMPLE
MgO FILLED EPOXY
COMBINED
CLOSURE PLUG
& BLOCK
FEEDTHROUGH
3.18
2.41

A short pulse of 30 nanosecond duration was obtained with approximately 2.5 nanosecond as the rise time. Typical voltage and current pulse shapes are shown in Fig. 2.5 (a and b). These pulses were obtained at a pressure equal to 6.2 kbars and 77K. In most cases the voltage pulses were quite smooth over the pulse length. However, in a few cases some ringing was observed, especially for high amplitude pulses.

2.2 The Hall Effect Measurements

The van der Pauw[16] technique was used to determine the specific resistivity ρ and carrier concentration n. All thermomagnetic effects except the Ettingshausan effect (which is negligible in any case) were eliminated from the Hall voltage reading by reversing the current and magnetic field and taking the appropriate averages. The four sample terminals were employed as indicated in the sketch below in order to measure the resistivity and Hall voltage.

Resistivity measurements:

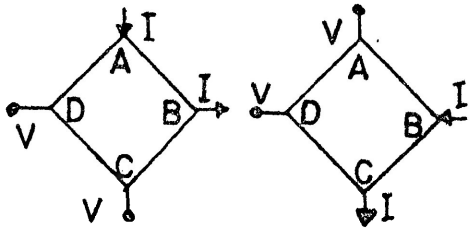

FIGURE 2.5a Current Pulses as a Function of Time at $P \simeq 6.2$ kbars and $T = 77K$.

FIGURE 2.5b Voltage Pulses as a Function of Time at $P \simeq 6.2$ kbars and $T = 77K$.

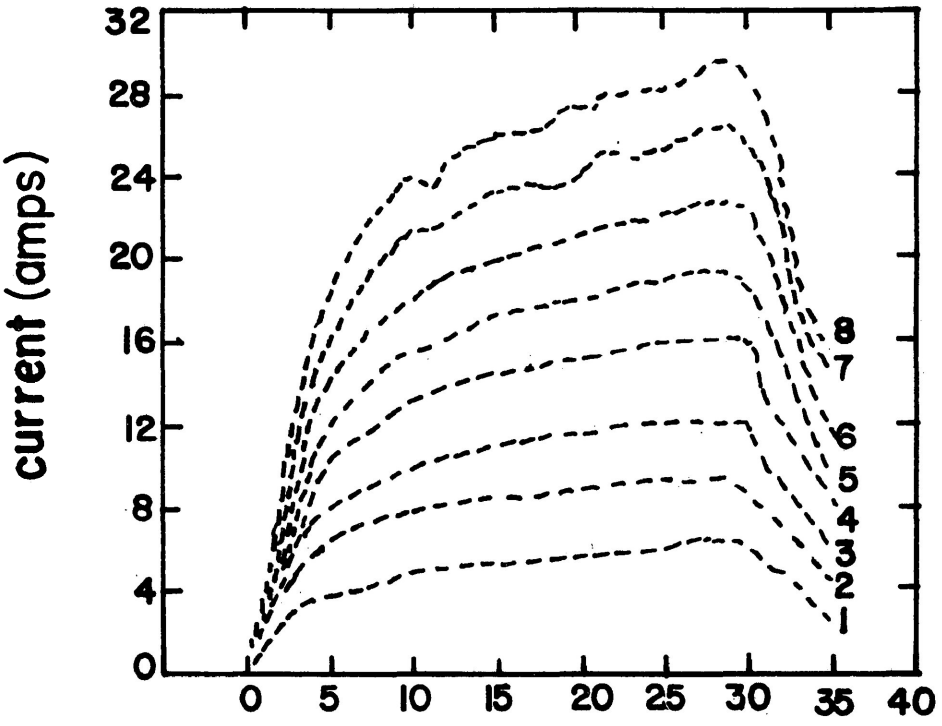
current (amps)
32
28
24
20
16
12
8
4
0
0
5
10
15
20
25
30
35
40
t (nsec)
8
7
6
5
4
3
2
1

(a)

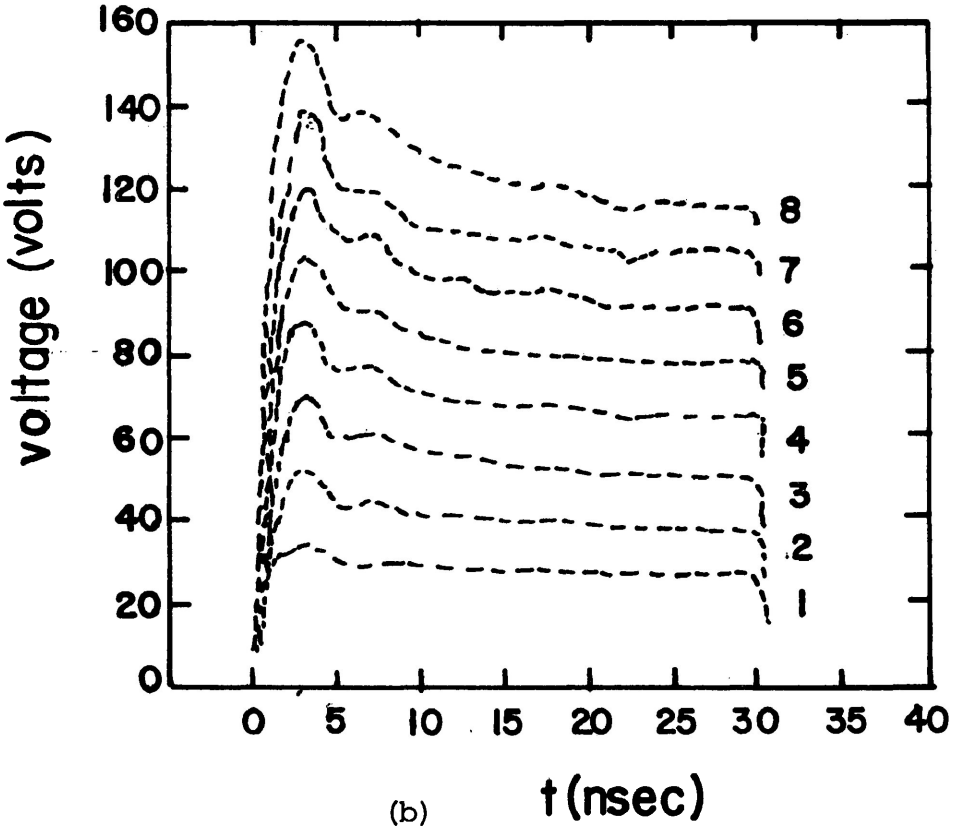
voltage (volts)
160
140
120
100
80
60
40
20
0
0
5
10
15
20
25
30
35
40
t (nsec)
8
7
6
5
4
3
2
1

(b)

Hall measurements:

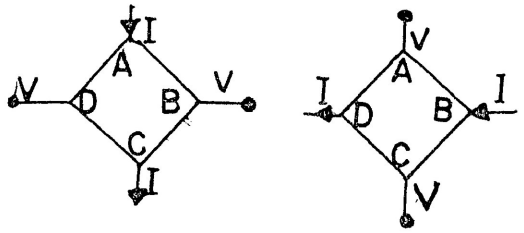

The van der Pauw expression for the specific resistivity is:

$$\rho = \frac{\pi d}{\ell n\ 2}\left(\frac{R_{AB,CD} + R_{BC,DA}}{2}\right) f\left(\frac{R_{AB,CD}}{R_{BC,DA}}\right) \qquad 2.1$$

where d is the sample thickness parallel to $\vec{B}$, and $R_{AB,CD}$, for example, is the potential difference between the contacts C and D per unit current through the contacts A and B.

The parameter f is a slowly varying function of the ratio $R_{AB,CD}/R_{BC,DA}$ only and satisfies the relation

$$\frac{R_{AB,CD} - R_{BC,DA}}{R_{AB,CD} + R_{BC,DA}} = f \text{ arc cosh } \left(\frac{\exp(\ell n\ 2/f)}{2}\right). \qquad 2.2$$

For ideal conditions $R_{AB,CD} \approx R_{BC,DA}$ and then f = 1.

This condition was achieved by making proper contacts.

Similarly, the carrier concentration n is given by:

$$n = \frac{|\vec{B}|}{ed} \left(\frac{1}{\Delta R}\right) \qquad 2.3$$

$$= \frac{|\vec{B}|}{ed} \frac{I}{V_H} \qquad 2.4$$

where $\Delta R = \Delta R_{AC,BD}$ is the sample resistance change due to the magnetic field $\vec{B}$ and

V_H = Hall voltage across the terminals A and C.

The carrier mobility was obtained from the relation,

$$\mu_H = 1/ne\rho. \qquad 2.5$$

Hall and resistivity measurements were made using the same pressure vessel as used in the Gunn effect study in a clamp mode so that the vessel could be removed from the press frame. The pressure vessel was then mounted on a closed cycle helium refrigerator capable of covering the temperature range from 300K to 64K. Additionally, the single lead pulse feed-through was replaced by a multiwire feed-through for making four lead measurements.

2.3 Sample Preparation

The samples were cut from a single crystal with a wire-saw employing a loop wire and a silicon carbide and oil slurry. The sample dimensions were 1 x 1 x 2.5 mm for the Gunn study and 1 x 1 x 0.4 mm for the Hall measurements. While cutting produced little damage, the sample was etched to provide a fresh surface. The etch used was CP4A which contains 25 ml HNO_3, 15 ml HF, and 25 ml CH_3 COOH. After etching, the sample was washed with methanol and trichloro ethylene. The sample was contacted using platinum wire and indium + 2% T_e solder. The platinum wires were then connected to the feed-through system. The sample was then enclosed in a Teflon capsule filled with a 1:1 mixture of isoamyl alcohol and n-pentane.

CHAPTER 3

RESULTS AND DISCUSSIONS

3.1 The Pressure Dependence of the Gunn Threshold

The electric field $\vec{E}$ vs current density j curves have been obtained at pressures up to 12 kbars from I vs t and V vs t pulses like those shown in Fig. 2.5. The current density rises sharply at the threshold electric field because of avalanching within the Gunn domain. This condition of carrier increase was used to define the threshold electric field. Figs. 3.1, 3.2, and 3.3 show E-j curves at 5 kbars, 9.2 kbars, and 10 kbars, respectively. The threshold field for several pressures is shown in Fig. 3.4. Note that the pressure vs E_{th} plot does not contain data between P = 0 and about 4.5 kbars. Since the sample resistance was less than 3 Ω in this pressure range, we were unable to maintain the required constant voltage condition at the sample necessary for defining E_{th}. The threshold electric field at zero pressure is available from previous measurements.[2,17]

A monotonic decrease in the threshold is observed up to a pressure of approximately 9 kbars. Thereafter, it gradually increases with increasing pressure. This is the behaviour reported

FIGURE 3.1 Current density vs electric field data for n-InSb at P = 5 kbars and T = 77K taken at different times after the leading edge of the pulse.

- 12 nanoseconds
- 16 nanoseconds
- 20 nanoseconds
- 24 nanoseconds
- 28 nanoseconds

The arrow marks the location of E_{th} while the bar is an estimate of uncertainty in its position.

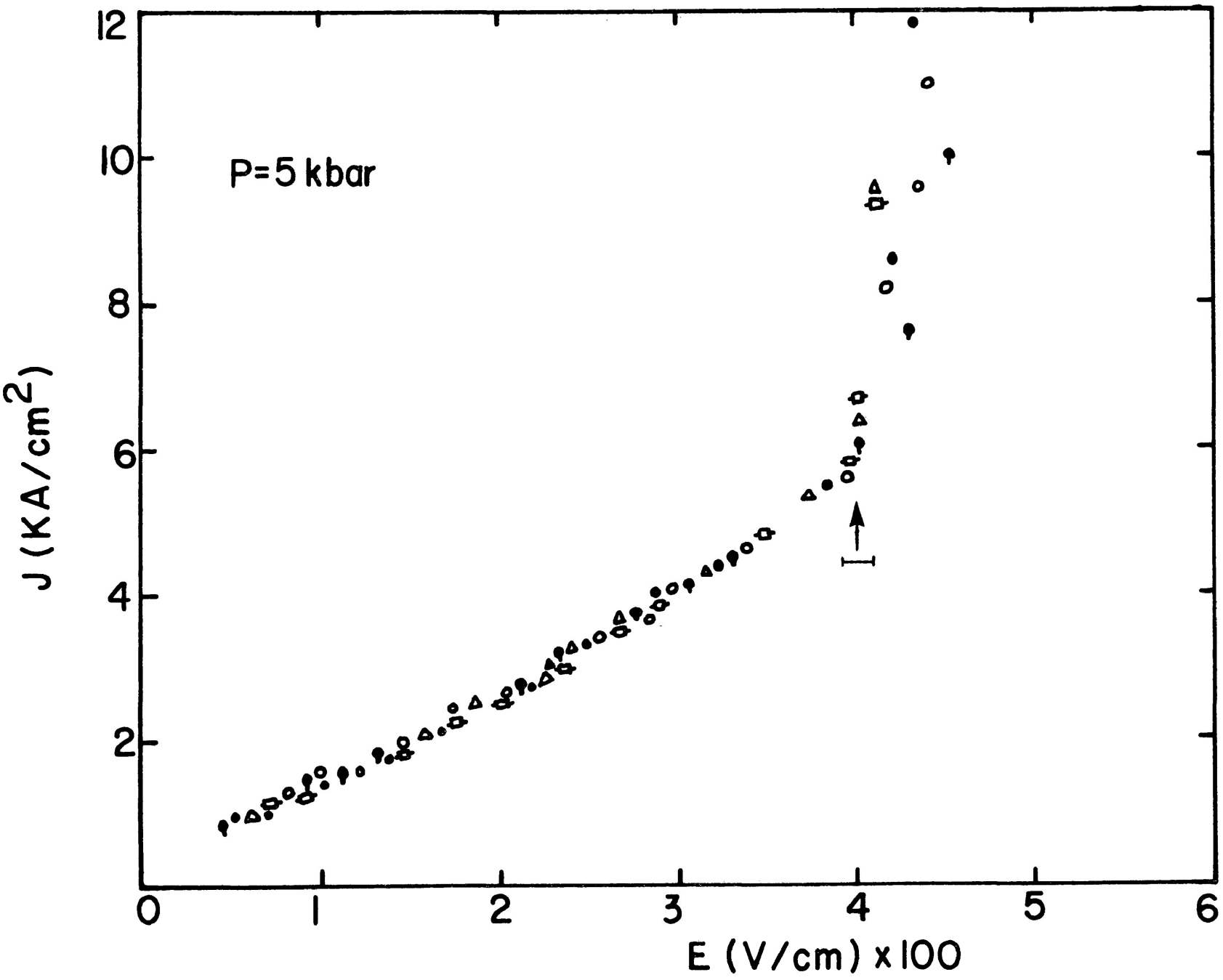
P=5 kbar
J (KA/cm²)
E (V/cm) x 100
0
1
2
3
4
5
6
2
4
6
8
10
12

FIGURE 3.2 Current density vs electric field data for n-InSb at P = 9.2 kbars and T = 77K taken at different times after the leading edge of the pulse.

8 nanoseconds

12 nanoseconds

16 nanoseconds

20 nanoseconds

24 nanoseconds

28 nanoseconds

The arrow marks the location of E_{th} while the bar is an estimate of uncertainty in its position.

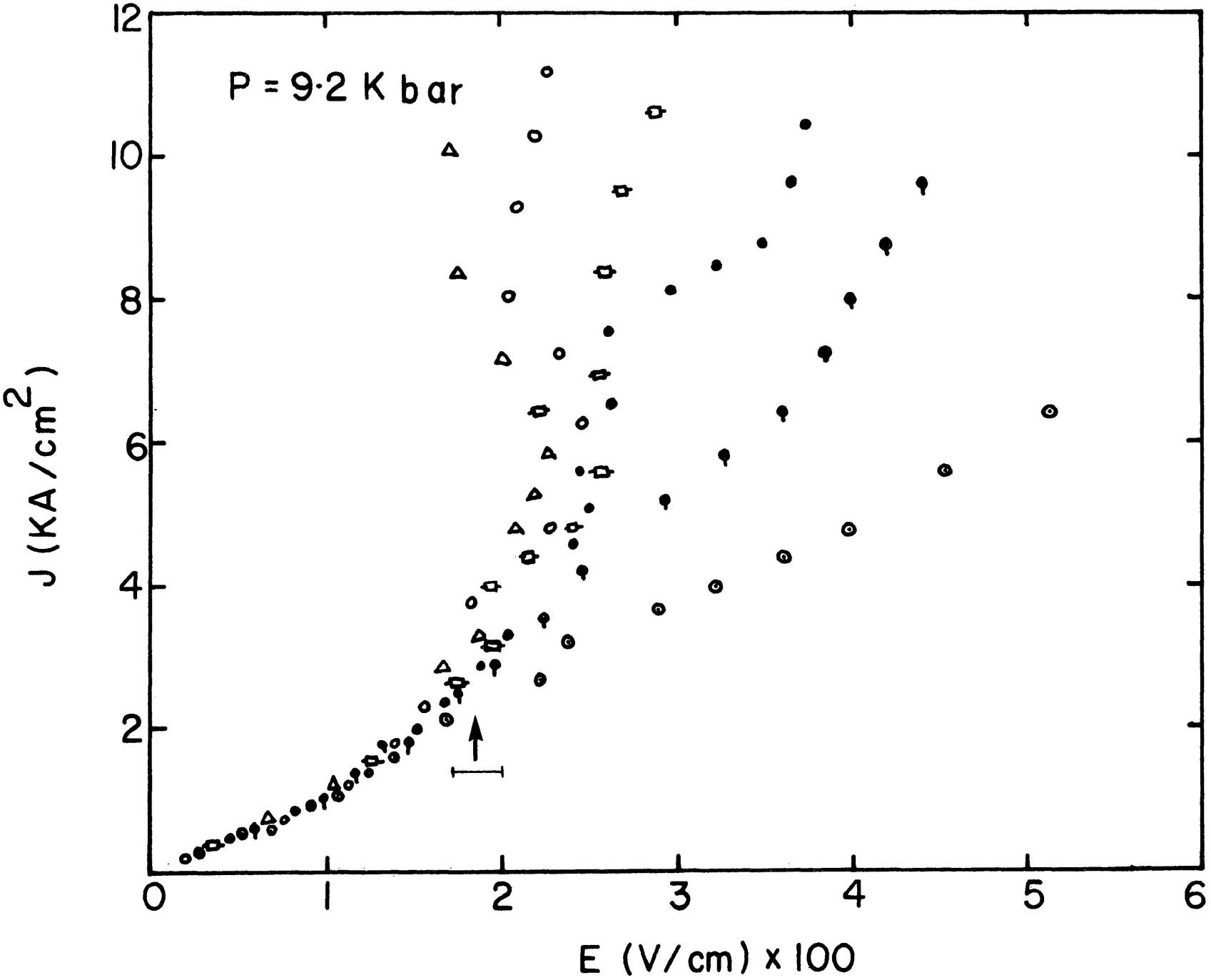
P = 9·2 K bar
J (KA/cm^2)
E (V/cm) x 100
0
1
2
3
4
5
6
2
4
6
8
10
12

FIGURE 3.3 Current density vs electric field data for n-InSb at P = 10 kbars and T = 77K taken at different times after the leading edge of the pulse.

- 8 nanoseconds
- 12 nanoseconds
- 16 nanoseconds
- 20 nanoseconds
- 24 nanoseconds
- 28 nanoseconds

The arrow marks the location of E_{th} while the bar is an estimate of uncertainty in its position.

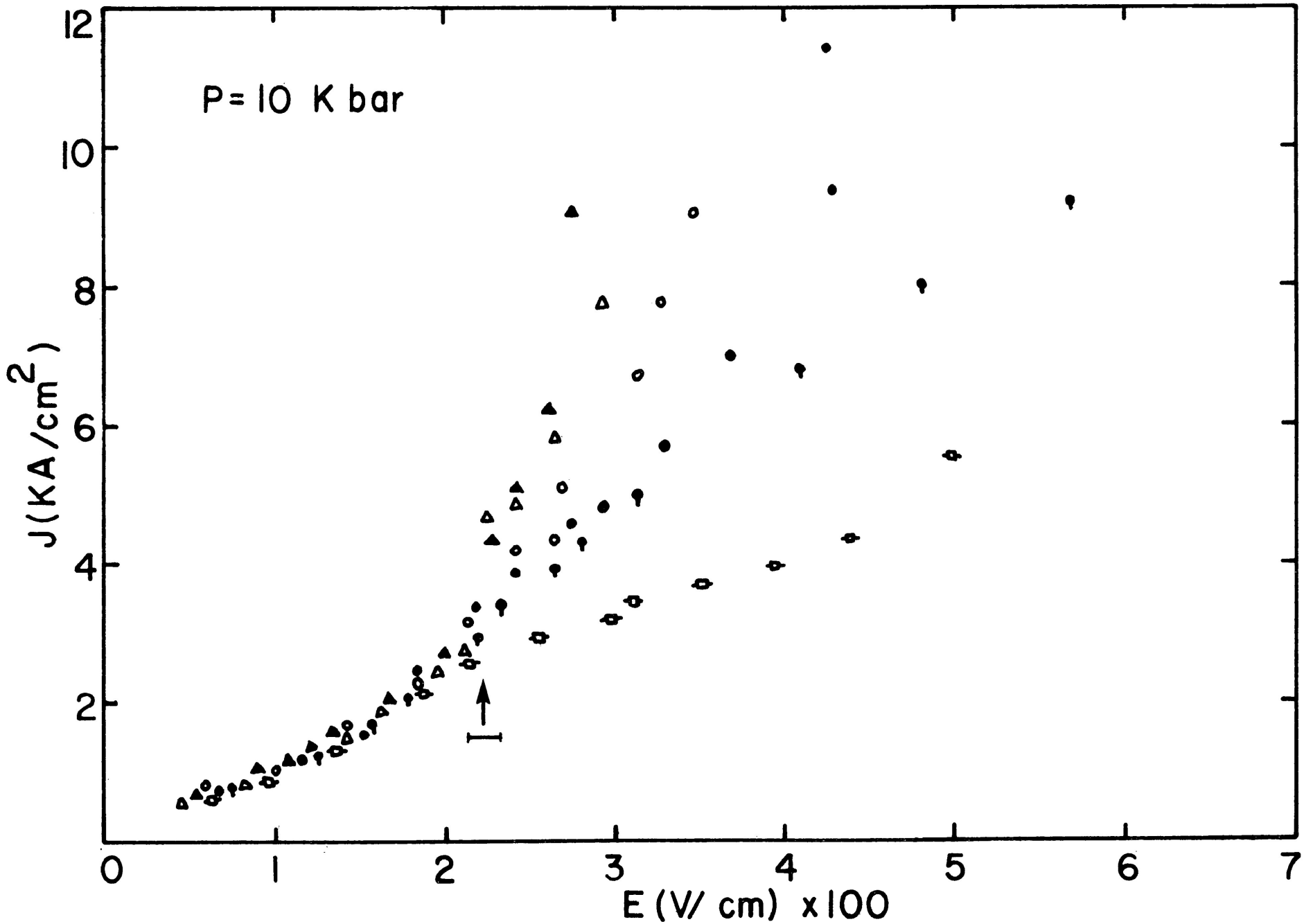
P= 10 K bar
J(KA/cm^2)
E (V/ cm) x100
0
1
2
3
4
5
6
7
2
4
6
8
10
12

by Porowski and co-workers for their type A samples. The samples investigated by Dobrovol'skis *et al.*[3] had a donor concentration and electron mobility very nearly equal to those studied here. They reported a monotonic decrease in E_{th}, similar to the B group of samples investigated by Porowski *et al.*[1] Two comments are in order here. The B group samples were reported to exhibit little change in carrier concentration with increasing pressure. In his work on magnetic freeze-out, Sladek[18] found that freeze-out only occurred for samples whose carrier concentration was less than approximately $10^{14}/cm^3$. For concentrations greater than this, the impurity electron orbits overlap so much that the impurities form a band even after the orbits have been reduced by a magnetic field (the cyclotron radius is less than the normal bound electron radius). If pressure produces freeze-out with a reduction in orbit radius, the B group samples probably have a higher concentration of donors and resist pressure freeze-out in the same way they resist magnetic freeze-out. The second comment concerns the method of determining the Gunn threshold by Dobrovol'skis *et al.*[3] Instead of obtaining I vs t and V vs t pulses they deduced sample resistivity by observing the pulses reflected off the sample due to miss-match at the end of the transmission line. This can be difficult because of the inevitable reactance at the pressure feed-through connection, and also because the sample resistivity increases by about 30 fold at 15 kbars. The

FIGURE 3.4 Threshold electric field E_{th} as a function of pressure, P at 77K. E_{th} has a shallow minimum at P ≃ 9.2 kbars. The P = 0 kbar point was obtained from the literature. The results displayed are for sample no. 2. The error estimates were obtained by considering both uncertainty in sample length and uncertainty in the position of the threshold field.

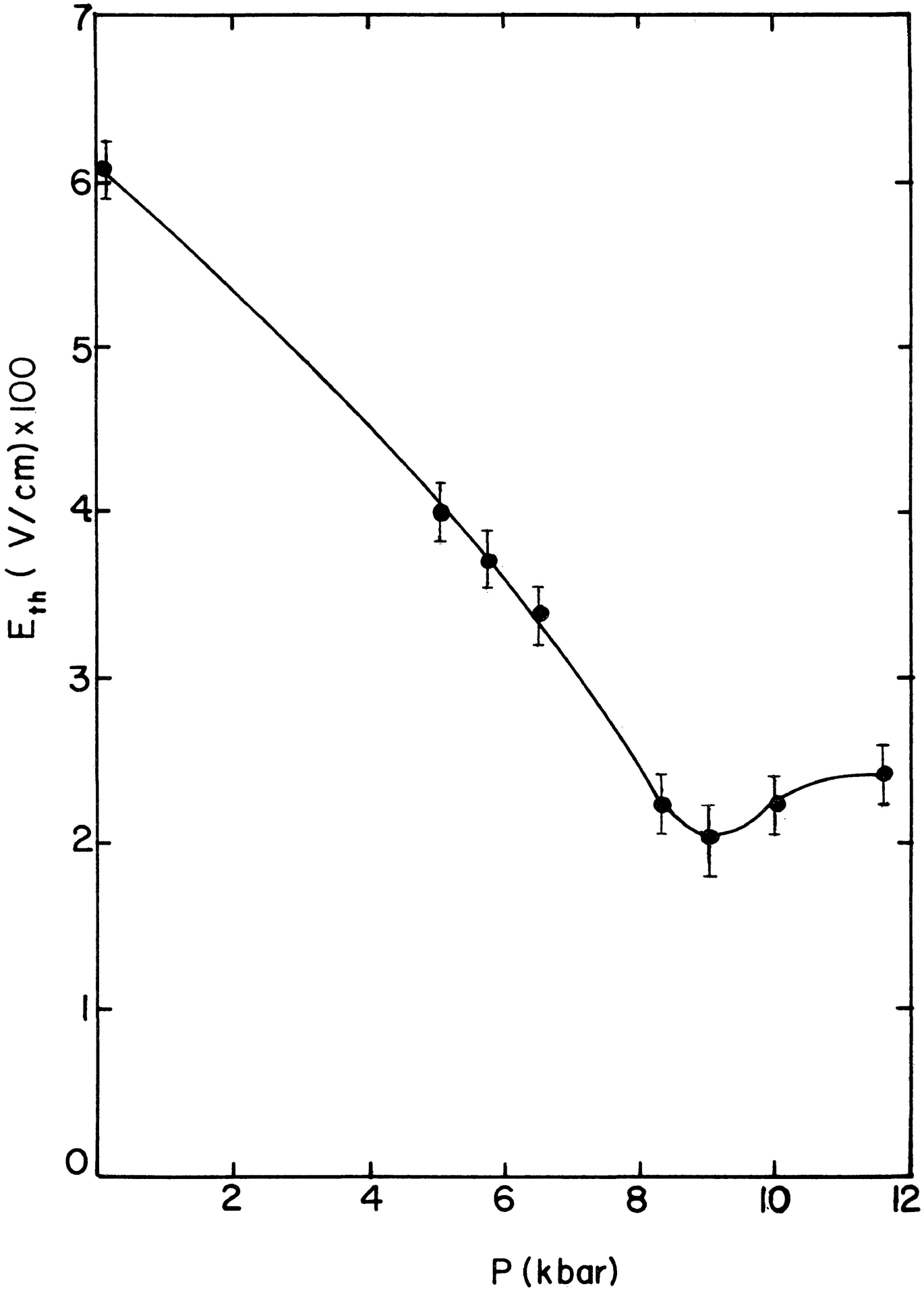
7
6
5
4
3
2
1
0
E_{th} (V/cm) x 100
2
4
6
8
10
12
P (kbar)

combination of changing load due to pressure and feed-through miss-match may have made the threshold minimum unresolveable.

3.2 The Pressure Dependence of the Resistivity

Using the van der Pauw relation for ρ (Eqn. 2.1) we have obtained resistivity vs pressure plots by pressurizing the sample at fixed temperatures of 296K, 198K, and 77K. These plots are shown in Figs. 3.5 and 3.6.

T = 296K:

The resistivity increases nearly exponentially with increasing pressure. When the pressure is reduced, hysteresis is observed. This is due to friction between the ½ hard anti-extrusion cap and the wall of the inner-pressure cyclinder. The hysteresis loop does not change even after cycling pressure several times and hence can be used for determining pressures to within approximately 4% at 296K.

FIGURE 3.5 Resistivity vs pressure for n-InSb at T = 296K. The hysteresis loop may be used to calibrate the pressure.

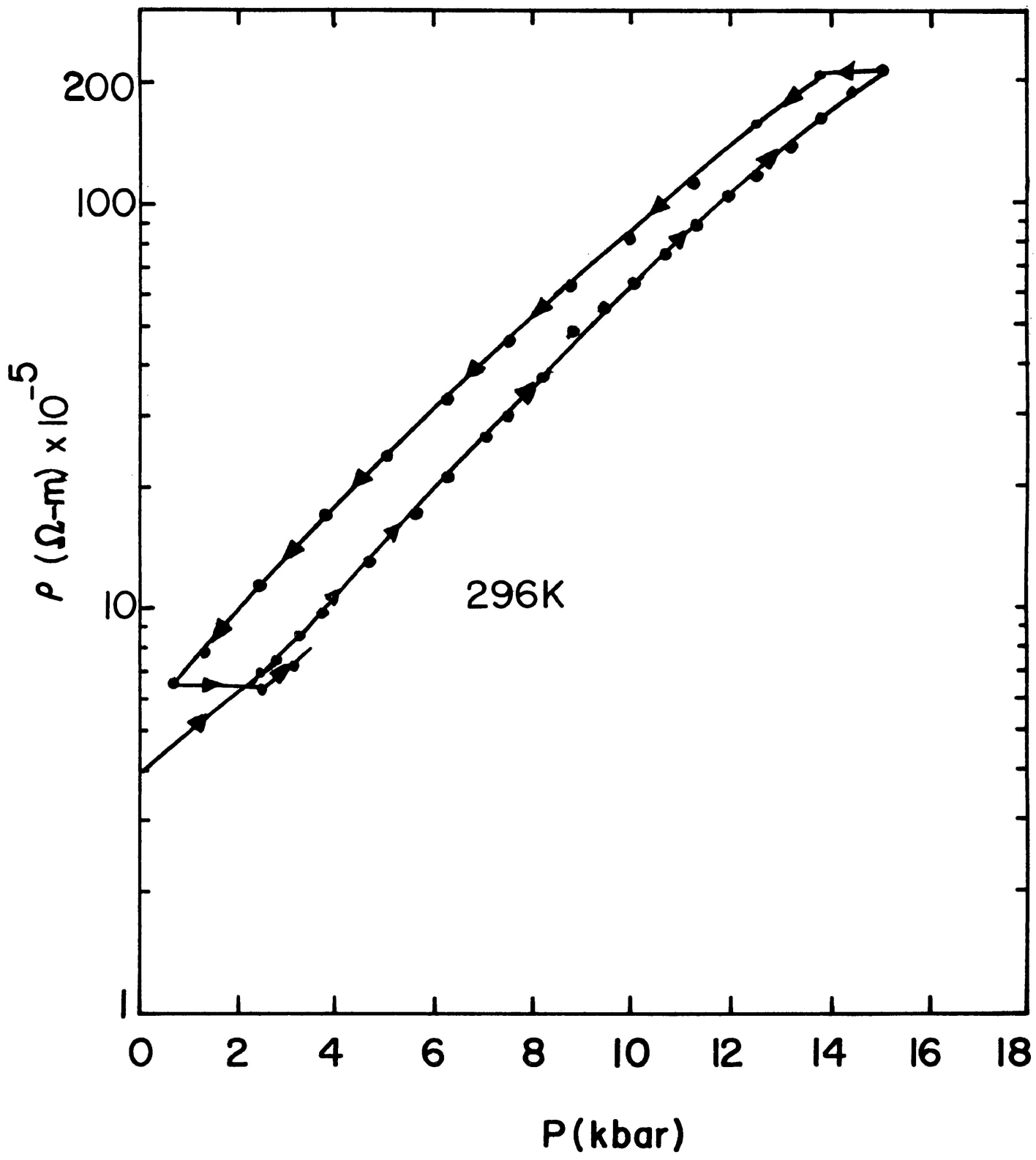
200
100
10
1
ρ (Ω-m) x 10^-5
296K
0
2
4
6
8
10
12
14
16
18
P(kbar)

FIGURE 3.6 Resistivity vs Pressure for n-InSb at T = 198K. and 77K. The resistivity increases very quickly at T = 77K and P $\simeq$ 10.5 kbars.

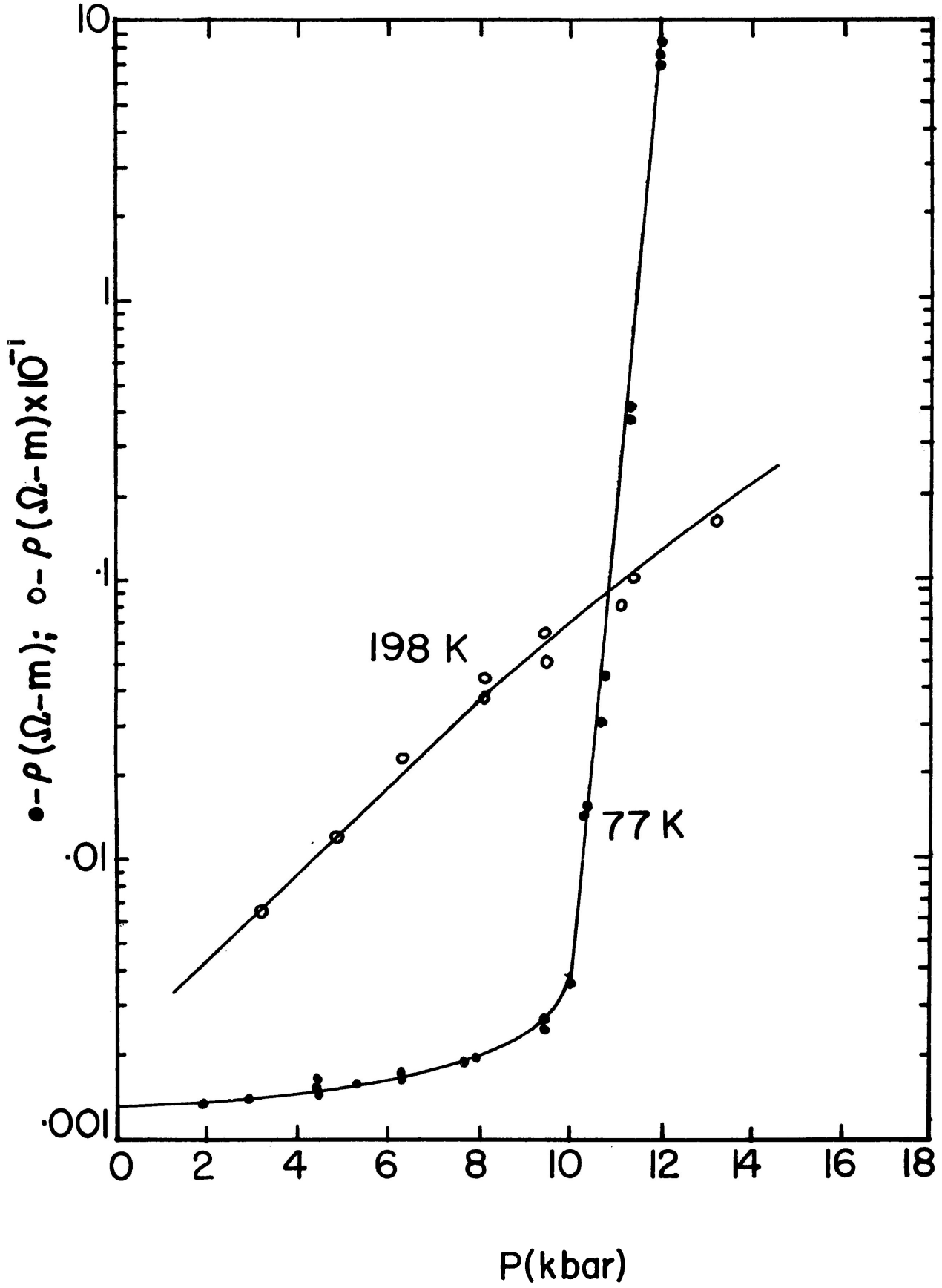
10
1
·1
·01
·001
•-ρ(Ω-m); ○-ρ(Ω-m)x10⁻¹
198 K
77 K
0
2
4
6
8
10
12
14
16
18
P(kbar)

T = 198K:

The resistivity varies exponentially with the pressure in a similar way to its behaviour at T = 296K because the sample is still intrinsic.

T = 77K:

Since the sample has become extrinsic, the resistivity varies only slowly with pressure up to approximately 10 kbars where it suddenly increases dramatically. This rise in the resistivity is due to carrier freeze-out into donor states which are becoming separated from the conduction band by a progressive increase in pressure. This freeze-out effect is discussed in section 3.3.

3.3 The Pressure Dependence of the Carrier Concentration

We used the following relation to determine the carrier concentration n:

$$n = \frac{|\vec{B}|}{ed} \left(\frac{1}{\Delta R}\right) .$$

The change in resistance ΔR was obtained in the following way: Since $\Delta R = I/V_H$, we set the current I to be constant and determined the Hall voltage from the relation:

$$V_H = V_{I^+,B^+} - V_{I^+,B^-} + V_{I^-,B^-} - V_{I^-,B^+}$$

where the signs on the subscript denote forward and reverse directions for current and magnetic field.

The plots for n vs P for fixed temperatures of 296K, 198K, and 77K are shown in Figs. 3.7 and 3.8.

T = 296K:

The carrier concentration decreases gradually with increasing pressure at T = 296K. When the pressure is reduced hysteresis is again observed. The decrease in n with increase in pressure is primarily responsible for the increase in the resistivity due to pressure. We may obtain dE_g/dP from knowledge of n vs P. Assuming $m_n^* \alpha E_g$ from Kanes theory (Eqn. 1.6) Equation 1.23 becomes:

$$\frac{d(\ell n\ n)}{dP} = \frac{3}{4}\ \frac{d(\ell n\ E_g)}{dP} - \frac{1}{2K_BT}\ \frac{dE_g}{dP}$$

$$= \frac{dE_g}{dP}\ \left(\frac{3}{4E_g(P)} - \frac{1}{2K_BT}\right)$$

where

$$E_g(P) = E_g(0) + \frac{dE_g}{dP}\ \delta P.$$

FIGURE 3.7 Carrier Concentration n vs P for n-InSb at T = 296K.

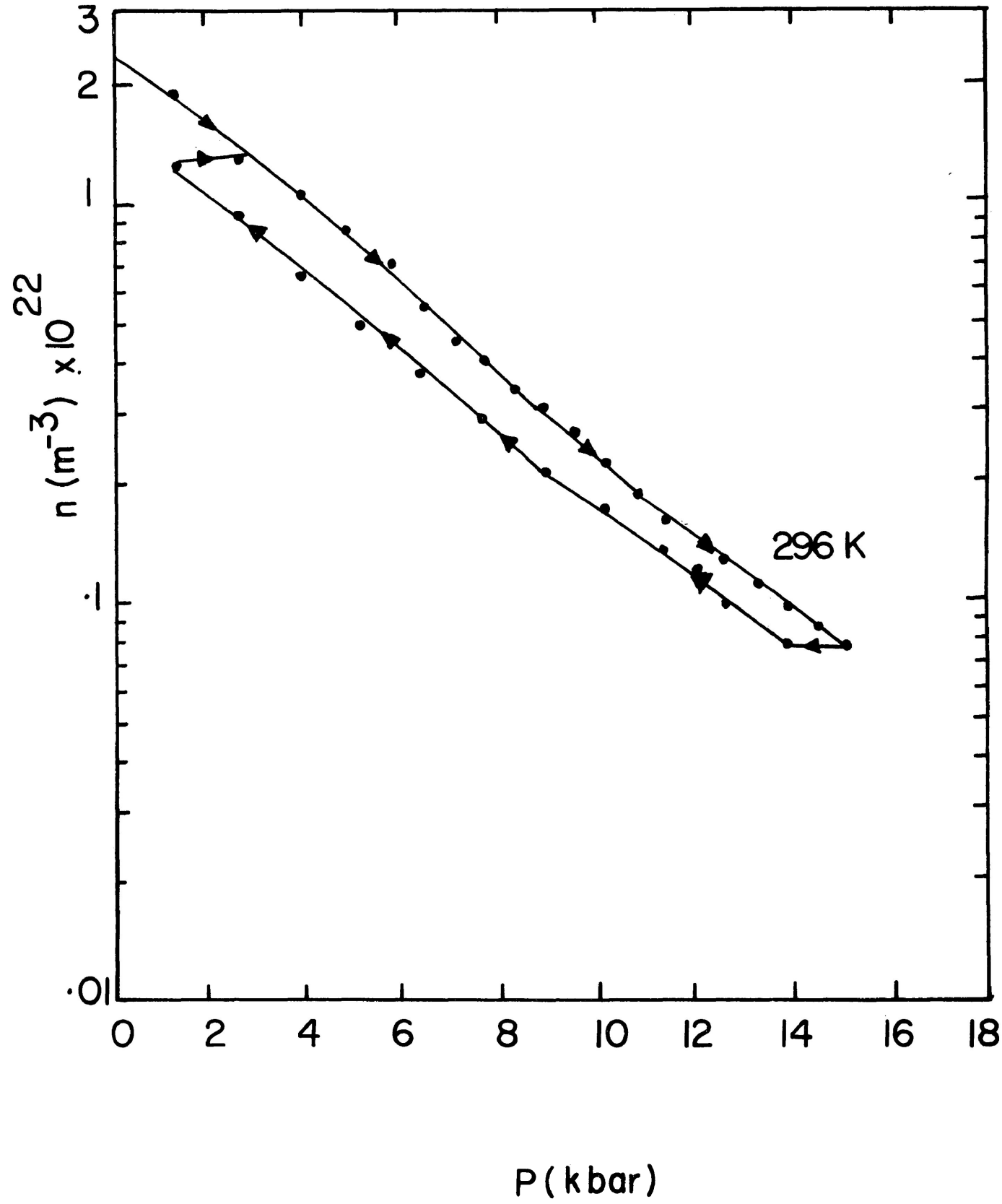
3
2
1
·1
·01
n (m^{-3}) x10^{22}
296 K
0
2
4
6
8
10
12
14
16
18
P (k bar)

Therefore,

$$\frac{dE_g(P)}{dP} = \frac{d(\ell n\ n)}{dP}\left(\frac{3}{4E_g(P)} - \frac{1}{2K_BT}\right)^{-1}$$

taking $E_g(0) = 0.18$ ev* at $P = 0$, estimating $d(\ell n\ n)/dP$ at $P = 0$, $P = 8$ kbars, and $P = 16$ kbars from Figure 3.7 and solving for dE_g/dP self-consistently, we obtain:

$$dE_g/dP = 15.5 \pm 0.2 \text{ mev/kbar at } P = 0$$

$$= 13.5 \pm 0.2 \text{ mev/kbar at } P = 8 \text{ kbars}$$

$$= 12.5 \pm 0.2 \text{ mev/kbar at } P = 16 \text{ kbars}$$

Thus dE_g/dP decreases with increasing pressure. We take as an average value $dE_g/dP = 14.0 \pm 0.2$ mev/kbar.

T = 198K:

At T = 198K the decrease in n is exponential which shows that the sample is in the intrinsic range.

---

*accepted zero pressure gap at room temperature.

FIGURE 3.8 Carrier Concentration n vs Pressure P for n-InSb at T = 198K and 77K.

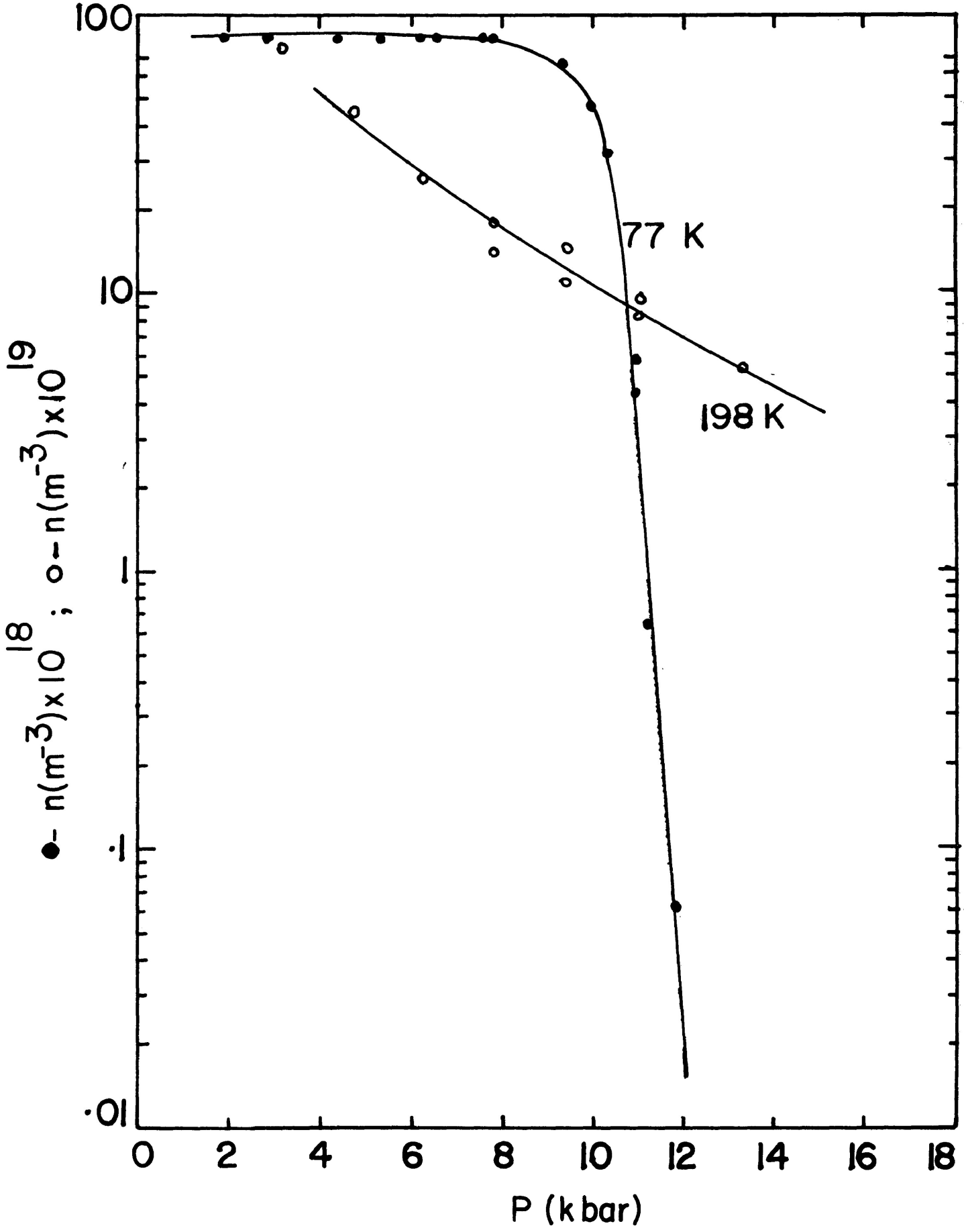
100
10
1
·1
·01
77 K
198 K
● - n(m⁻³)x10¹⁸ ; o - n(m⁻³)x10¹⁹
0
2
4
6
8
10
12
14
16
18
P (k bar)

T = 77K:

The carrier concentration is constant up to a pressure of approximately 10 kbars. However, carrier concentration decreases very rapidly at higher pressures. This rapid decrease in n is due to carrier freeze-out.

To determine the donor ionization energy E_D, we held pressure constant and varied temperature in the low temperature extrinsic range. From the experimental data and Eqn. 1.27, the value of E_D is obtained. Fig. 3.9 shows the value of E_D for several pressures. For pressures less than about 4 kbars the donor band overlaps the conduction band and no discernible gap is obtained. Since E_D is increasing at an exponential rate, as soon as it becomes appreciable with respect to K_BT, the carrier density in the conduction band decreases rapidly with increasing pressure and/or decreasing temperature.

3.4 The Pressure Dependence of E_g

The zero temperature energy gap E_g (P) is obtainable from the slope of a semilogarithmic plot of $(n/T^{3/2})$ vs 1/T (see Eqn. 1.22). Carrier concentration n was determined from Hall measurements for several pressures over the temperature range 305K

FIGURE 3.9 Donor Energy Gap E_D vs Pressure P. E_D varies approximately exponentially with Pressure. T = 77K.

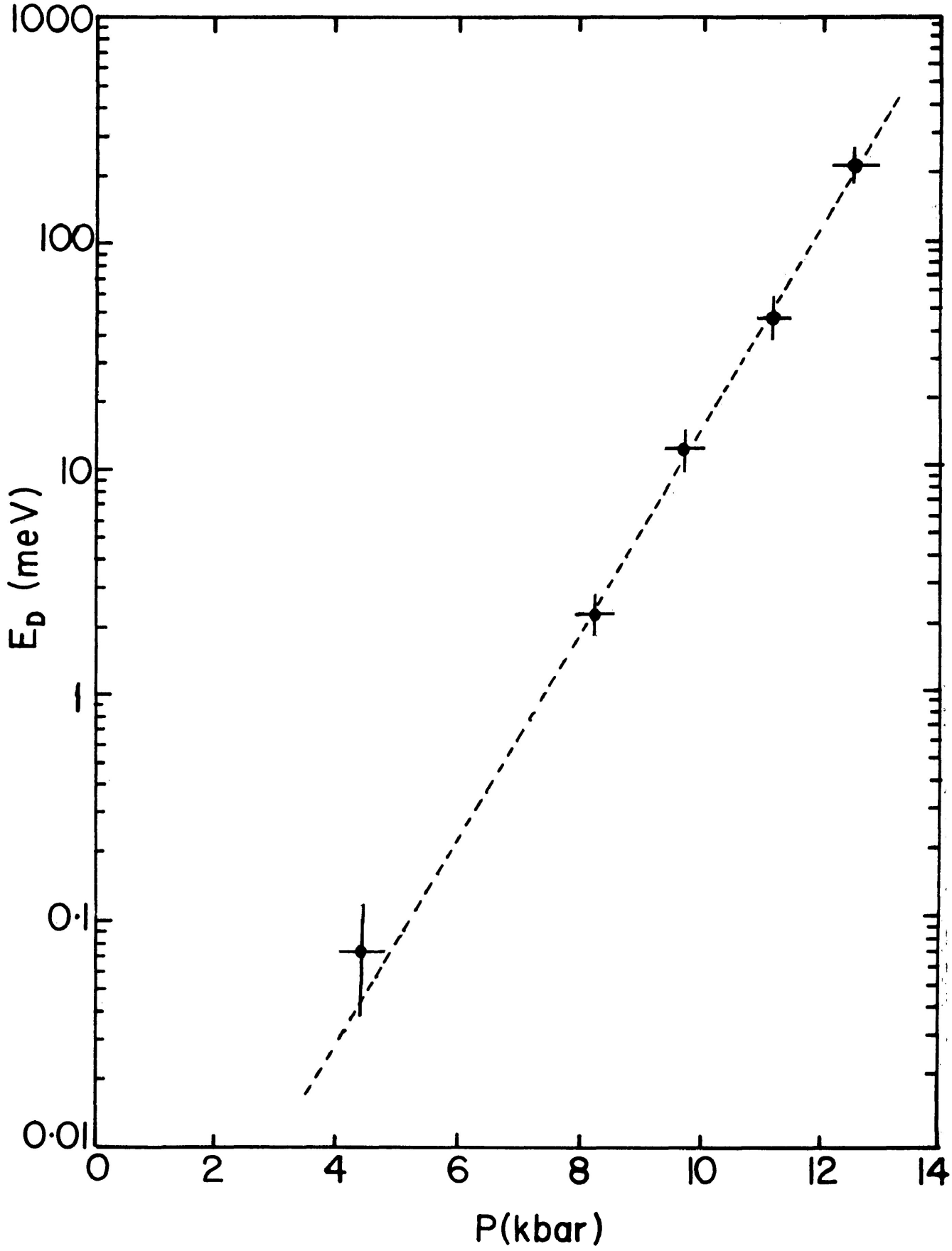
1000
100
10
1
0·1
0·01
E_D (meV)
0
2
4
6
8
10
12
14
P(kbar)

to 285K. Fig. 3.10 shows E_{go} vs P. From this graph we obtain dE_{go}/dP equal to 13.9 ±0.4 mev/kbar for the 0 - 6 kbars and 13.0 ±0.5 mev/kbar from the higher pressure range. These results are in good agreement with the values obtained in section 3.3 on the pressure dependence of n. As before the derivative seems to decrease with an increasing pressure. It should be noted that these are constant pressure varying temperature results while the previous results were obtained for constant temperature and varying pressure. Since dE_{go}/dP and dE_g/dP are so close it seems safe to assume that the temperature coefficient α is insensitive to pressure.

Our value of dE_g/dP is in good agreement with that of Long,[6,19] (dE_g/dP = 14.2 ±0.3 mev/kbars). The measurement of Keyes[20] is somewhat higher at 15.5 ±1 mev/kbar but is based on resistivity measurements only, which means there is some problem in deciding what $d\mu/dP$ should be. In contrast, Long's value was determined using Hall measurements for n, and his pressure medium was helium which is very hydrostatic. However, he only went to 2 kbars in pressure. Bradley and Gebbie[21] estimated dE_g/dP at 16 ±1 mev/kbar using optical absorption. This seems outside the range of our results. They used solid pyrophyllite as a pressure transmitting medium in a cubic anvil device and the polished samples were sandwiched between rock salt disks. Their results may be influenced by the non-hydro static pressure resulting from this type of apparatus.

FIGURE 3.10 The Energy Gap E_{go} versus Pressure

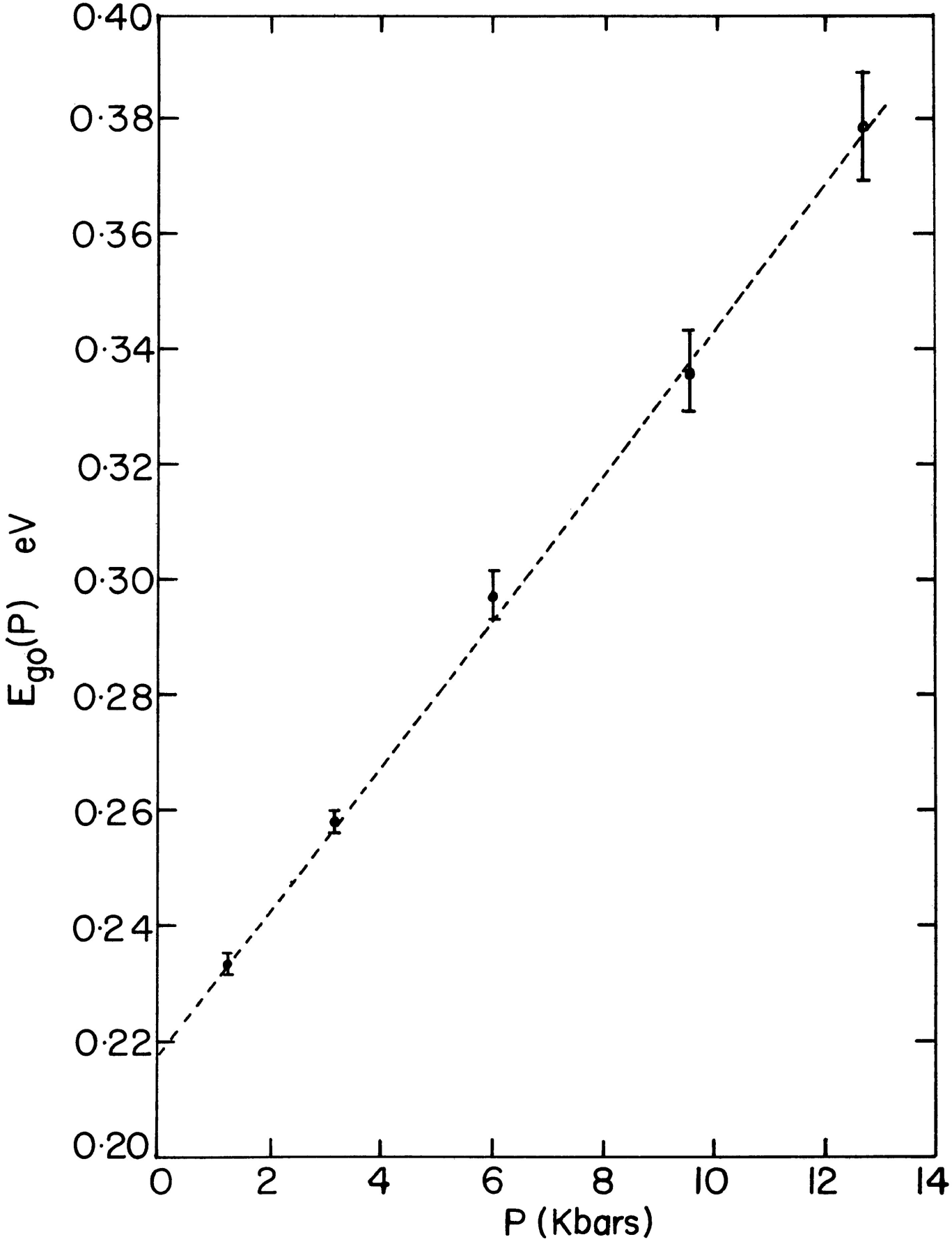
0·40
0·38
0·36
0·34
0·32
0·30
0·28
0·26
0·24
0·22
0·20
$E_{go}(P)$ eV
0
2
4
6
8
10
12
14
P (Kbars)

CHAPTER 4

CONCLUSION

In undoped n-InSb with a low impurity concentration ($n \sim 8 \times 10^{13}$ cm^{-3}) the Gunn threshold electric field was found to decrease with increasing pressure in two separate samples. The threshold passed through a minimum at P ≃ 9.2 kbars and then increased gradually as pressure increased to ∿ 12 kbars. For the low pressure region:

$$\frac{d\,|\vec{E}_{th}|}{dP} = -46.2 \text{ volts/meter-kbar.}$$

From an estimate of $\frac{dE_{\Gamma L}}{dP}$ = -6 mev/kbar one may obtain:

$$\frac{d\,|\vec{E}_{th}|}{dE_{\Gamma L}} = 7.7 \text{ volts/meter-mev.}$$

The increase in $|\vec{E}_{th}|$ for pressures greater than 9 kbars is thought to be due to carrier freeze-out. The threshold increases because the field must first ionize donor atoms before transfering electrons from the Γ to L conduction band. This behaviour is similar to that reported by Porowski *et al.*[2] for his group A samples.

Dobroval'skis *et al.*[3] reported a monotonic decrease in the Gunn threshold for essentially identical sample material as used for this study. One possible explanation for the disagreement lies in their method of determining the Gunn threshold field.

In addition to the Gunn threshold study an investigation of impurity ionization energy has been carried out using Hall measurements. For a low impurity concentration, the ionization energy increases approximately exponentially with pressure. In the region of freeze-out, the donor electrons are probably localized to the region of a single impurity atom. For higher donor impurity concentrations the donor electron wave functions probably overlap at higher pressure and a donor band should still exist. Further investigations of the process of carrier freeze-out as a function of donor concentration therefore are indicated.

The pressure dependence of the intrinsic gap E_g also was determined. The derivative dE_g/dP decreases with increasing pressure. The low pressure value obtained is in good agreement with the value obtained by Long[6]. At 12 kbars the magnitude of the derivative is about 10% lower than the zero pressure value.

REFERENCES

1. Sylvester Porowski, William Paul, J.C. McGroddy, Marshal I. Nathan, and J.E. Smith, Solid State Communication, 7, 905 (1969).

2. John E. Smith, J. Marshal, I. Nathan, James C. McGroddy, Sylvester A. Porowski, and William Paul, Applied Physics Letters, 15, 242 (1969).

3. Z. Dobrovol'skis, A. Krotkus, K. Repshas and Yu. Pozhela, Sov. Phys. Semicond., 10, 478 (1976).

4. E.O. Kane, J. Phys. Chem. Solids, 1, 249 (1957).

5. W.M. Coderre and J.C. Woolley, Can. J. Physics, 47, 2553 (1969).

6. D. Long and P.H. Miller, Jr., Phys. Rev. 98, 1192 (1955).

7. Y.F. Tsay and S.S. Mitra, Phys. Rev., B10, 1476 (1974).

8. C.H. Hilsum, Proc. IRE, 50, 185 (1962).

9. K. Seeger, Semiconductor Physics, p. 41, Springer-Verlag, New York, Wien (1973).

10. J.C. Blackmore, Semiconductor Statistics, p. 96, Pergamon Press (1962).

11. Madelung, O., H. Weiss, Z. Naturforsch, 99, 527 (1954).

12. K. Seeger, Semiconductor Physics, p. 46, Springer-Verlag, New York, Wien (1973).

13. R.E. Jones, Jr., G.C. Anderson, and W.J. Keeler, Rev. Sci. Instrum., 46, 1025 (August, 1975).

14. Walter C. Johnson, Transmission Lines and Networks, p. 90, McGraw-Hill Book Co., N.Y. (1950).

15. R.E. Jones, Jr. and W.J. Keeler, Rev. Sci. Instrum., 46, 1028 (August, 1975).

REFERENCES continued....

16. L.J. van der Pauw, Philips Research Reports, 13, No. 1, February, 1958.

17. W.J. Keeler, Lakehead University, Canada, Private Communication.

18. R.J. Sladek, Phys. Chem. Solids, Pergamon Press, 5, 157 (1958).

19. D. Long, Phys. Rev., 99, 388 (1955).

20. R.W. Keyes, Phys. Rev., 99, 490 (1955).

21. C.C. Bradley and H.A. Gebbie, Phys. Letters, 16, 109 (1965).